Nanoscale

Accepted Manuscript

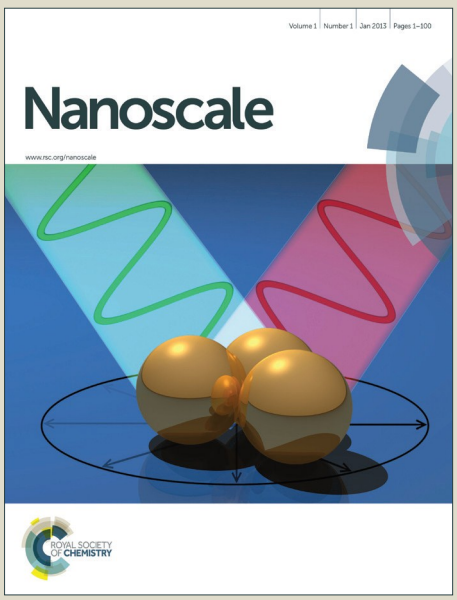

ROYAL SOCIETY OF CHEMISTRY

www.rsc.org/nanoscale

Journal Name

RSCPublishing

ARTICLE

Core-shell hybrid upconversion nanoparticles carring stable nitroxide radicals as potential multifunctional nanoprobes for upconversion luminescence and magnetic resonance dual-modality imaging

Cite this: DOI: 10.1039/x0xx00000x

Received 00th January 2012,
Accepted 00th January 2012

DOI: 10.1039/x0xx00000x

www.rsc.org/

Chuan Chen, [a] Ning Kang, [b] Ting Xu, [a] Dong Wang, [ab] Lei Ren[*b] and Xiangqun Guo[*a]

Nitroxide radicals, such as 2,2,6,6-tetramethylpiperidine 1-Oxyl (TEMPO) and its derivatives, have recently been used as contrast agents for magnetic resonance imaging (MRI) and electron paramagnetic resonance imaging (EPRI). However, their rapid one-electron bioreduction to diamagnetic N-hydroxy species when administered intravenously has limited their use in *in vivo* applications. In this article, a new approach of silica coating for carrying stable radicals was proposed. 4-Carboxyl-TEMPO nitroxide radical was covalently linked with 3-aminopropyl-trimethoxysilane to produce a silanizing TEMPO radical. Utilizing a facile reaction based on the copolymerization of silanizing TEMPO radical with tetramethy orthosilicate in reverse microemulsion, a TEMPO radicals doped SiO_2 nanostructure was synthesized and coated on the surface of $NaYF_4$:Yb,Er/$NaYF_4$ upconversion nanoparticles (UCNPs) to generate a novel multifunctional nanoprobe, PEGylated UCNP@TEMPO@SiO_2 for upconversion luminescence (UCL) and magnetic resonance dual-modality imaging. The electron spin resonance (ESR) signals, generated by the TEMPO@SiO_2 show an enhanced reduction resistance property for a period of time up to 1 h even in the present of 5 mM ascorbic acid. The longitudinal relaxivity of PEGylated UCNPs@TEMPO@SiO_2 nanocomposites is about 10 times stronger than that for free TEMPO radicals. The core-shell $NaYF_4$:Yb,Er/$NaYF_4$ UCNPs synthesized by a modified user-friendly one-pot solvothermal strategy show a significant enhancement of UCL emission up to 60 times than the core $NaYF_4$:Yb,Er. Furthermore, the PEGylated UCNP@TEMPO@SiO_2 nanocomposites were further used as multifunctional nanoprobes to explore the performance in the UCL imaging of living cells and T_1-weighted MRI *in vitro* and *in vivo*.

Introduction

As the development of medical science and technology in the recent years, early diagnosis and treatment of diseases is becoming more and more desirable than before. Single imaging technique used for diagnosis, including magnetic resonance imaging (MRI), ultrasound, X-ray computed tomography (CT), positron emission tomography (PET), single-photon emission CT (SPECT) and optical imaging technologies, is usually insufficient to provide enough information for precise early medical diagnosis and effective therapy of various diseases. To overcome this shortage and incorporate the advantages of different imaging tools, increasing attention has been focused on developing multimodal nanoprobes using combined imaging modalities. One of the frequently reported dual-modal nanoprobes is fabricated by integrating MRI contrast agent and fluorescence probe in a single nanocomposite, which can simultaneously provide the excellent three-dimensional (3D) anatomical and functional information of soft tissues and the high resolution and sensitivity of imaging at the cellular level.[1-4]

The most commonly used fluorescence moieties for MRI/fluorescence dual-modal nanoprobes are organic dyes and semiconductor quantum dots (QDs). However, organic dyes and QDs are downconversion phosphors, the excitation wavelength of them are generally within the ultraviolet light or blue light region. This will lead to strong autofluorescence background, low penetration depth and damage to biological samples when using them as bioimaging probes. Besides, the photobleaching of organic dyes and the toxicity of QDs also constraint the development of their practical applications as imaging probes. As an alternative to conventional fluorescent probes, lanthanide-doped upconversion nanoparticles (UCNPs) show strong upconversion luminescence (UCL) emission in the near infrared (NIR) or visible range upon irradiation with NIR light. Since the "optical

transmission window" of most bio-species is located in the NIR range (750-1000 nm), the use of UCNPs in bioimaging have special advantages including low autofluorescence background, deep tissue penetration and reduced photodamage.[5-9] Considering such valuable advantages, UCNPs are increasingly used as a bioprobe module in multi-modality imaging.[10-12] Co-doping of Gadolinium (Gd^{3+}) in the rigid structure of UCNPs is a straightforward strategy to construct dual-modal nanoprobes for UCL/MR dual-modality imaging,[13-20] due to the high paramagnetism property of Gd^{3+}. However, Gd^{3+} ions doped deeply inside of the UCNPs have less chance to efficiently exchange the magnetic fields with surrounding water protons than those on the surface of nanoparticles.[21] Meanwhile, excessive co-doping of Gd^{3+} ions is easy to cause a quenching of upconversion fluorescence due to the change of host matrix.[22] Thus, core-shell $NaYF_4$:Yb, Er/$NaGdF_4$ nanocrystals were synthesized to improve its longitudinal relaxivity and upconversion luminescence intensity, although it takes a high level of skill to precisely control the thickness of $NaGdF_4$.[23] Another strategy to get Gd-UCNPs multi-modality bioprobe is to attach the Gd-DTPA complex to the surface of UCNPs.[24, 25] However, even for chelated Gd^{3+}-complexes, the release of the metal ion *in vivo* during metabolic processes and the potential toxicity are pertinent issues, which may cause the fears and concerns of patients.[13] Besides of Gd-based UCNPs, superparamagnetic iron oxide nanoparticles (IONPs) have also been assembled with UCNPs to fabricate multifunctional nanoprobes for UCL/MR imaging.[26, 27] However, these IONP-UCNP nanocomposties usually exhibit the reduced UCL intensity because the light of excitation and emission could be partially absorbed by the IONPs to some extent.[4] Therefore, it is still challenging and desirable to find some suitable alternatives of Gd-based UCNPs and IONP-UCNP nanocomposties to develop multifunctional nanoprobes for UCL/MR dual-modality imaging.

Nitroxide radicals, such as 2,2,6,6-tetramethylpiperidine 1-Oxyl (TEMPO), are a class of stable, non-toxic organic molecules which have a single unpaired electron. Due to their unique paramagnetic property, they have long been used as spin labelling agents for electron spin resonance (ESR) imaging or as contrast agents for MRI.[28, 29] In combination with site-directed spin labeling (SDSL), nitroxide radicals are also well-known as powerful ESR-sensitive probes to study concentration, structure, dynamics, and interactions of various analytes.[30-32] Because of their ability to participate in cellular redox reactions, nitroxide radicals have also been used as spin probes to monitor redox status *in vivo*.[33, 34] As a class of potential MRI contrast-enhancing agents, nitroxide radicals show obviously advantage because of their lower toxicity in comparison with the conventional MRI contrast agents (e.g., gadolinium derivatives). However, nitroxide radicals are sensitive to the reduction status of biological samples.[29, 33, 35] Their rapid *in vivo* reduction to the corresponding diamagnetic hydroxylamines can lead to a significantly loss of ESR signal and MRI relaxation time. It has been demonstrated that half-life of free TEMPO radicals in blood was about 15 s, which was far from satisfactory for practical use.[36] To solve this issue, numerous efforts have been made to enhance the stability of nitroxide radicals by the encapsulation or functionalization of nitroxide radicals into polymers,[37-41] lipid emulsion,[42] DNA oligomers,[43] single-walled carbon nanotubes,[44] and albumin.[45] However, it still has been challenging to achieve spin labeled contrast agent with good anti-reduction performance under *in vivo* applications.

Silica coating, chemically and thermally inert against the degradation in biological environment, has been a frequently used technique for surface modification of nanoparticles in biomedical applications.[46] This coating method can protect the core nanoparticles against the external environment, thereby improving the stability and biocompatibility of the nanoparticles. Moreover, the silica coated surface of nanoparticles can be further functionalized by biomolecules or ligands with amines, thiols and carboxyl groups.

Inspired by these premises, herein, TEMPO radicals doped paramagnetic silica layer was coated onto $NaYF_4$:Yb, Er/$NaYF_4$ nanoparticles to construct multifunctional nanoprobes for UCL/MR dual-modality imaging. The as-prepared nanocomposites were labeled as UCNP@TEMPO@SiO_2, which was further functionalized with poly (ethylene glycol) (PEG) to improve the colloidal stability and biocompatibility. The paramagnetic TEMPO@SiO_2 layer was formed by copolymerization of a paramagnetic precursor (derived from 3-aminopropyltrimethoxysilane (APTS)) with tetraethyl orthosilicate (TEOS). The paramagnetic precursor was obtained by coupling APTS with 4-Carboxy-TEMPO. Moreover, this compact inert shell of SiO_2, acted as a protection barrier, can protect the doped TEMPO radicals from being reduced to the corresponding hydroxylamines by small reducing substances, such as glutathione and ascorbic acid. To the best of our knowledge, this is the first study reporting the novel combination of UCNPs with TEMPO nitroxide radicals for UCL/MR dual-modality imaging. The longitudinal relaxivity of PEGylated UCNP@TEMPO@SiO_2 nanocomposites is about 10 times stronger than that of free nitroxide radicals. MTT assay reveals low cytotoxicity of PEGylated UCNP@TEMPO@SiO_2 nanocomposites. This multifunctional nanoprobe was used for the *in vitro* UCL bioimaging under 980 nm infrared laser excitation. In addition, both of the T_1-weighted MRI in aqueous and HeLa cells suspension showed the contrast brightening increased with the concentration of PEGylated UCNP@TEMPO@SiO_2 nanocomposites, which revealed that a satisfied MRI contrast performance of this multifunctional nanoprobe could be obtained. Finally, *in vivo* T_1-weighted MRI show the enhancement of MR signals in the livers of mice administered with these nanocomposites. These results indicate that the PEGylated UCNP@TEMPO@SiO_2 nanocomposites present potential for UCL/MR dual-modality imaging applications.

Experimental

2.1 Materials

Anhydrous YCl_3 (99.99 %), anhydrous $YbCl_3$ (99.9 %), anhydrous $ErCl_3$ (99.9 %) were purchased from National Engineering Research Centre of Rare Earth Metallurgy and Function Materials (Baotou, China). NaOH (> 98 %), NH_4F (> 98 %), 1-octadecene (ODE, 90 %), oleic acid (OA, 90 %), 2-ethoxy-1-ethoxycarbonyl-1,2-dihydroquinoline (EEDQ) were purchased from Alfa Aesar Co., Ltd (Shanghai, China). Poly-oxyethylene (5) nonylphenylether (Igepal CO-520), 3-aminopropyltriethoxylsilane (APTS), tetraethyl orthosilicate (TEOS), fluorescein isothiocyanate (FITC) and 4-Carboxy-TEMPO were purchased from Sigma-Aldrich Co., Ltd (Shanghai, China). mPEG-NHS was purchased from Sinopeg Biotech Co., Ltd (Xiamen, China). Unless otherwise noted, all chemicals were used as received without further purification. Milli-Q water (18.2 MΩcm) was used in all experiments.

2.2 Synthesis of TEMPO@SiO_2 nanoparticles

The core-shell TEMPO@SiO_2 nanoparticles were prepared by reverse microemulsion approach. Firstly, the silanizing TEMPO radical precursors were prepared by the reaction of 4-Carboxy-TEMPO with APTS, which is similar to that reported previously.[47, 48] A solution of 22.5 μL of APTS and 24 mg of 4-Carboxy-TEMPO with 60.8 mg of EEDQ in methanol (1 mL) was allowed to stand for 24 h at room temperature. After removing methanol via reduced pressure distillation, the product was redissolved in 2 mL of water. After ultrasonic dispersion, 150 μL of the solution was mixed with 750 μL of water for further use. TEMPO@SiO_2 was synthesized using a cyclohexane/Triton X-100/n-hexanol/water water-in-oil (w/o) reverse

microemulsion system. Briefly, cyclohexane (16.8 mL), Triton X-100 (4 mL), n-hexnol (4 mL) were mixed and stirred thoroughly for 10 min, then 150 μL of the as-prepared silanizing TEMPO radical precursors solution was added with continuously stirring for over 5 minutes. Next, the container was sealed and sonicated for 1 h until a transparent emulsion was formed. 60 μL of ammonia (wt 30%) was then added into the solution, the solution was rotated for 24 h. Thereafter, 100 μL of TEOS were added and the solution was stirred for 12 h. Finally, TEMPO@SiO_2 were precipitated by adding 20 mL of acetone, and the nanoparticles were washed with acetone and ethanol and dried under vacuum at room temperature.

2.3 Synthesis of core $NaYF_4$: Yb,Er UCNPs

Monodisperse $NaYF_4$:Yb,Er UCNPs were synthesized by a user-friendly one-pot solvothermal strategy using NH_4F-NaOH-Re-OA as shell precursors. Typically, 0.4 mmol YCl_3, 0.09 mmol $YbCl_3$ and 0.01 mmol $ErCl_3$ in methanol were added to a 100 mL three-neck flask containing 3 mL of OA and 7.5 mL of ODE. The solution was heated to 130 °C under argon flow with constant stirring for 30 min to form a clear yellow solution, and then cooled down to room temperature. 5 mL of methanol solution containing NaOH (0.05 g) and NH_4F (0.074 g) was added and the solution was stirred for 60 min. After methanol evaporated, the solution was heated to 300 °C under argon for 1 h and cooled down to room temperature. The obtained UCNPs were precipitated from the solution by adding an equal volume of acetone. The mixed solution was centrifuged at 12000 rpm for 30 min. The precipitate was then redispersed in cyclohexane/ethanol/water (2:1:1) solution. The solution was gently mixed and allowed to stand until the cyclohexane layer did not show any turbidity. The cyclohexane layer containing UCNPs was extracted, then the solvent was removed via reduced pressure distillation. The resulted UCNPs with a yield about 70 mg were redispersed in cyclohexane as stock solution (10 mg/mL).

2.4 Synthesis of core-shell $NaYF_4$:Yb,Er/$NaYF_4$ UCNPs

The synthesis of the core/shell UCNPs were prepared via a modified successive layer-by-layer injection protocol. Y-OA precursor: A mixture of YCl_3 (1.75 mmol), OA (5 mL) and ODE (12.5 mL) was added in flask and heated to 130 °C under vacuum with magnetic stirring for 30 min to form colorless solution before cooling down to 90 °C for the following injection. NaOH-NH_4F-OA precursor: Firstly, a mixture of OA (5 mL), ODE (12.5 mL), 17.5 mL of methanol solution containing NaOH (0.175 g) and NH_4F (0.259 g) were mixed in a flask. After methanol was evaporated, the solution was heated to 120 °C to remove residual water and oxygen before cooling down to 90 °C for the following injection. The synthesis of core UCNPs was conducted as described above, after reacting for 60 min at 300 °C. Then 0.5 mL of Y-OA precu mgrsors and 0.5 mL of NaOH-NH_4F-OA precursors were successively injected into the reaction mixture and the ripening time between each injection was kept at 15 min. Each injection of shell precursors and ripening cycles represented a layer growth. The injection could be performed to 15 cycles and 30 cycles to get the core/shell UCNPs with 15 layers and 30 layers, respectively. The resulted core/shell UCNPs were collected and washed by the same method as mentioned above.

2.5 Synthesis of UCNP@TEMPO@SiO_2 nanocomposites

UCNP@TEMPO@SiO_2 nanocomposites were synthesized using a cyclohexane/CO-520/water water-in-oil (w/o) reverse microemulsion system. 0.45 mL of CO-520, 2 mL of cyclohexane and 1 mL of 10 mg/mL $NaYF_4$:Yb,Er/$NaYF_4$ solution in cyclohexane were mixed and stirred for 15 min, 50 μL of ammonia (wt 30%) were added dropwise, the container was sealed and sonicated for 1 h until a transparent emulsion was formed. The silanizing TEMPO radical precursors in methanol (1 mL) was condensed to 100 μL. Then, 50 μL of silanizing TEMPO radical precursors in methanol was added into the reverse microemulsion solution. The solution was magnetic stirred (600 rpm) for 12 h. After that, 20 μL of TEOS and 3 μL of APTS was added and the reaction was kept for another 12 h. Finally, the nanoparticles were obtained by centrifugation and washed with ethanol/water (1:1) thoroughly and then stored in deionized water.

2.6 Synthesis of PEGylated UCNP@TEMPO@SiO_2 nanocomposites

Briefly, the purified UCNP@TEMPO@SiO_2-NH_2 (20 mg) nanoparticles were dispersed in 4 mL of DMF, 20 mg of mPEG-NHS was added for PEGylation of nanoparticles. After 12 h reaction, the PEGylated UCNP@TEMPO@SiO_2 nanocomposites were collected by centrifugation and washed with deionized water for several times and then stored in deionized water.

2.7 Characterization

Powerder X-ray diffraction (XRD) was performed on AXS D8 advance (Bruker, Germany). Transmission electron microscopy (TEM) images were obtained using JEM-1400 (JEOL, Japan). High-resolution TEM (HRTEM), selected-area electron diffraction (SAED), Energy-dispersive X-ray (EDX) analysis were performed on TECNAI F-30 (FEI, Netherlands). X-ray photoelectron (XPS) measurements were performed on PHI Quantum 2000 XPS system (ULVAC-PHI Inc., Japan). Upconversion luminescence emission spectra were collected on a FluoroMax-4 spectrometer (Jobin Yvon Horiba, France) equipped with the excitation of an external 0-2 W adjustable 980 nm CW laser (Beijing Hi-tech Optoelectronic Co., China). Dynamic light scattering (DLS) and Zeta potential distribution were measured on Malvern Zetasizer Nano ZS (Malvern, UK). The upconversion luminescence (UCL) imaging was performed on a modified Nikon Ti-S inverted fluorescence microscope (Nikon, Japan) equipped with an external 980 nm CW laser (Beijing Hi-tech Optoelectronic Co., China). The MR T_1 relaxation and MR T_1-weighted imaging measurements were performed on a 9.4T MR scanner (Bruker 94/20, Germany). Flow cytometry analysis was performed on a BD Accuri C6 flow cytometer (BD Biosciences, USA). ESR measurements were performed using a Bruker EMX X-Band ESR spectrometer (Bruker, Germany). All microwave parameters were kept constant: 9.8 GHz microwave frequency, 2.0 mW microwave power, 10 dB attenuator, 100 kHz modulation frequency, 1.0 G modulation amplitude, and 0.64 ms time constant. The Fourier Transform Infrared Spectrometer (FTIR) spectra were recorded on Nicolet iS10 (Thermo Scientific, USA). The concentration of samles was fixed via the measurement of the Yb^{3+} contents in each sample by inductively coupled plasma atomic emission spectroscopy (ICP-AES).

2.8 Cell culture and cytotoxicity assay

HeLa cells were kind gift from Medical College of Xiamen University. Cells were cultured in DMEM (Dulbecco's Modified Eagle Medium) medium supplemented with 10% FBS, 1% penicillin/streptomycin and 2 mM L-glutamine, at 37 °C in a 5% CO_2 humidified atmosphere. The *in vitro* cytotoxicity was measured by using a 3-(4,5-dimethylthiazol-2-yl)-2,5-diphenyltetrazolium bromide (MTT) assay on HeLa cells. According to the typical procedure, HeLa Cells were seeded into a 96-well culture plate at 1×10^4/well and cultured in 5% CO_2 at 37 °C for 24 h. Then cells were subsequently incubated with various concentrations (6.25, 12.5, 25, 50, 100, 200 and 400 μg/mL, diluted in DMEM) of PEGylated UCNP@TEMPO@SiO_2 nanocomposites for 6 h or 24 h. Thereafter, the cells were washed with phosphate-buffered saline (PBS) for three times and incubated with MTT solution (1 mg/mL) at 37 °C in 5% CO_2 for 4 h. After the growth

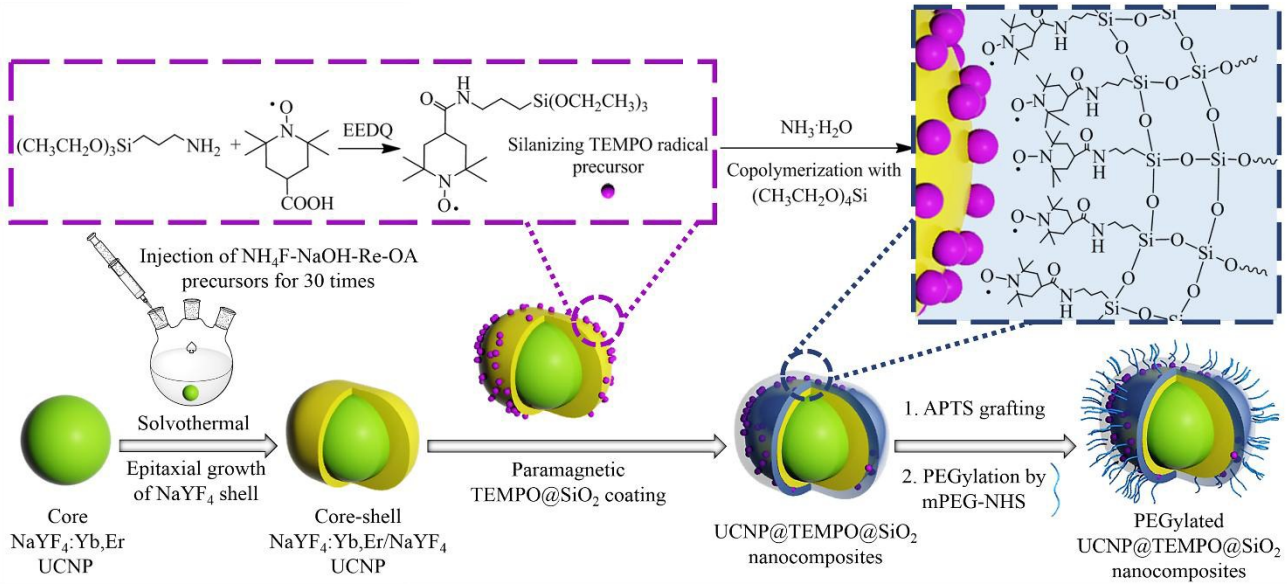

Scheme 1 Schematic illustration for the synthesis of PEGylated UCNP@TEMPO@SiO_2 nanocomposite

medium was removed, 100 μL of dimethyl sulfoxide (DMSO) was added in each well followed by incubation for another 30 min. Finally the absorbance of the resulted solution was measured at 570 nm using a microplate reader (BioRad 680, Hercules, CA, USA). The cell viability was displayed in percentage of control samples.

$$\text{Cell viability}(\%) = [A]_{sample}/[A]_{control} \times 100\%$$

Where $[A]_{sample}$ is the absorbance of formazan product in treated cells and $[A]_{control}$ is the absorbance of formazan in untreated cells.

2.9 Cellular uptake assay

The cellular uptake of PEGylated UCNP@TEMPO@SiO_2 was analyzed by flow cytometry. The as-prepared UCNP@TEMPO@SiO_2-NH_2 nanocomposites were labeled with FITC and mPEG-NHS. Briefly, 25 mg of UCNP@TEMPO@SiO_2-NH_2 were dispersed in 20 mL of DMF, then, 20 mg of mPEG-NHS was added. The solution was magnetic stirred (600 rpm) for 12 h. After that, certain amount of FITC was added and stirred overnight. The resulted FITC-labeled PEGylated UCNP@TEMPO@SiO_2 was centrifuged, washed with ethanol for several times. HeLa cells were cultured into 12-well plates at 1×10^5/well and incubated with samples (0, 8, 15, 30, 60, 125 μg/mL) at 37 °C in 5% CO_2 for 6 h, and then washed with PBS sufficiently to remove excess nanocomposites. After that, the cells were collected by trypsinization and suspended in PBS. Cells incubated in the absence of the UCNPs were used as control. The amounts of samples taken up by cells were measured using FL-1 channel. FACS data were analyzed using Flow Jo (7.6 versions).

2.10 Upconversion luminescence bioimaging *in vitro*.

Upconversion luminescence imaging was performed on an inverted fluorescence imaging microscope (Nikon Ti-S) equipped with an external CW 980 nm laser as the excitation source. An 850 nm short-pass filter was placed before the CCD to cut the excitation light. HeLa cells grown on coverslips (1×10^5/well) were incubated with PEGylated UCNP@TEMPO@SiO_2 (0, 40, 80, 120, 160, 200 μg/mL) at 37 °C in 5% CO_2 for 6 h. After washed with PBS for three times, the cells were also stained with Hoechst 33258 (50 μg/mL) for 30 min to show the nuclei as blue. After washing with PBS again for three times, the upconversion luminescent signals were collected at 500-560 nm with 3 s of exposure by 20x objective lens.

2.11 MRI of PEGylated UCNP@TEMPO@SiO_2 *in vitro*.

The MR T_1 relaxation and MR T_1-weighted imaging measurements were performed on a 9.4 T MR scanner (Bruker 94/20, Germany). Firstly, different amount of PEGylated UCNP@TEMPO@SiO_2 nanocomposites were prepared in a series of equal volume of aqueous solution with 1% of agarose gel in 200 μL PCR tubes (0, 0.313, 0.625, 1.25, 2.5, 5 mg/mL) for MR T_1 relaxation and MR T_1-weighted imaging measurements. Secondly, HeLa cells were incubated with different concentrations (0, 40, 80, 120, 160, 200 μg/mL) of PEGylated UCNP@TEMPO@SiO_2 nanocomposite for 6 h. The labeled cells were washed with PBS, then collected by trypsinization and suspended respectively in a series of equal volume of DMEM culture media with 1% of agarose gel in 200 μL PCR tubes before MR T_1 relaxation measurement. The unlabeled cells were used as the control group.

2.12 MRI of PEGylated UCNP@TEMPO@SiO_2 *in vivo*

Animal experiment procedures were in agreement with the protocol approved by Institutional Animal Care and Use Committee of Xiamen University. For *in vivo* MRI studies, the nude mice was anesthetized by intraperitoneal injection of sodium pentobarbital (40 mg/kg). In order to raise the signal to noise ratio, a commercially available volume coil (RF RES 1H 75/40 Q TR, Germany) with 40 mm diameter was used. After intravenous injection of PEGylated UCNP@TEMPO@SiO_2 nanoparticles (200 μL, 0.5 mg/mL), the coronal and transversal cross section MR imaging were performed on a 9.4T MR scanner (TR = 1500 ms, TE = 8.5 ms, FOV 4 cm × 4 cm, slice thickness 1 mm). The MR images were obtained at baseline (prior to injection) and at 30 min post-injection. The animals were then removed from the MR scanner and allowed to recover.

Results and discussion

PEGylated UCNP@TEMPO@SiO_2 nanocomposites were constructed by the novel combination with homogenous active core–inert shell UCNPs and nitroxide radicals. As shown in Scheme 1, the

synthetic procedures for PEGylated UCNP@TEMPO@SiO_2 nanocomposites were divided into three steps. Firstly, uniformly sized active core–inert shell $NaYF_4$:Yb,Er/$NaYF_4$ with strong UCL emission was synthesized by a user-friendly one-pot solvothermal strategy using NH_4F-NaOH-Re-OA as shell precursors. Thereafter, 4-Carboxyl TEMPO was conjugated with APTS to get a silanizing TEMPO radical. For transferring the hydrophobic UCNPs to aqueous solution, the paramagnetic TEMPO@SiO_2 layer was coated on the surface of UCNPs by copolymerization with the silanizing TEMPO radical and TEOS via a reverse microemulsion method. Finally, in order to increase colloidal stability and biocompatibility, mPEG-NHS was linked with the amino-functionalized SiO_2 on the surface of UCNP@TEMPO@SiO_2. These as-prepared PEGylated UCNP@TEMPO@SiO_2 nanocomposites could serve as effective multifunctional nanoprobes for UCL/MR multi-modal bioimaging.

3.1 Synthesis and characterization of TEMPO@SiO_2 nanoparticles

Firstly, we took TEMPO@SiO_2 nanoparticles as model to test that whether the compartmentalization of the TEMPO radicals in the core of SiO_2 nanoparticles can enhance the stability of their ESR signal under reduction environment. The silanizing TEMPO radical precursors were obtained by a coupling reaction which have advantages of high yield. 4-Carboxy-TEMPO was conjugated to APTS in the presence of EEDQ, yielding the desired silanizing TEMPO radical (Scheme 1). This successful conjugation was confirmed by the measurement of FITR (Fig. S1†) and ESI-MS (Fig. S2†). Then, the paramagnetic TEMPO@SiO_2 nanoparticles were synthesized by copolymerization of silanizing TEMPO radicals with TEOS in reverse microemulsion. As shown in Fig. S3,† the obtained TEMPO@SiO_2 nanoparticles are roughly spherical with an average diameter of 33.5 ± 2.4 nm. The ESR signals of the obtained silanizing TEMPO radical precursors (Fig. S4a†) and TEMPO@SiO_2 nanoparticles (Fig. S4b†) were then analyzed by ESR measurement. The ESR spectrum of silanizing TEMPO radical precursors shows the expected three ^{14}N hyperfine lines, which are characteristic of freely-tumbling TEMPO radicals in solution. Moreover, the high-field line is slightly weaker than the others, indicating the slower tumbling rate of TEMPO molecule, due to covalent attachment with APTS moiety (Fig. S4a†). In contrast, the ESR spectrum of TEMPO@SiO_2 nanoparticles exhibits distinct anisotropy as evidenced by the broader line-width and the weaker high-field line than that of silanizing TEMPO radicals (Fig. S4b†). Fig. S5† shows the formation process of paramagnetic silica network structure, in which the silanizing TEMPO radicals stay at a very close distance to each other. The restriction of the mobility of TEMPO radicals embedded into rigid SiO_2 network structure can lead to a broadening of the ESR line-width and to a lower relative intensity of the high field signal,[37, 49] possibly due to the slower molecular tumbling. Furthermore, the high population of TEMPO radicals, which stay at a very close distance to each other in this self-assembling SiO_2 structure, may also lead to the broadness of ESR lines, due to the spin-spin interaction.[37, 50] In addition, no noticeable ESR signal was observed in supernatant after centrifugation of the solutions of TEMPO@SiO_2 (Fig. S4c†). In order to further prove that the TEMPO radicals were covalently attached into the SiO_2 nanoparticles, we carried on the control experiments by simply mixing the APTS and 4-Carboxy-TEMPO as precursors during the co-hydrolysis process. Without the covalent linkage between APTS and 4-Carboxy-TEMPO, TEMPO radicals may only adhere to SiO_2 nanoparticles by physical adsorption. After several times of centrifugation and washing, no ESR signal could be observed in the final product of SiO_2 nanoparticles (Fig. S4d†). The results of these control experiments show that the ESR signal of TEMPO@SiO_2 was originated from the TEMPO radicals covalently immobilized within the SiO_2 nanoparticles, instead of that encapsulated by physical adsorption.

As mentioned above, nitroxide radicals are sensitive to the reduction environment of biological systems. The antioxidants such as acorbic acid (Vc) and glutathione (GSH) are vital to keep the redox status in living cells and widely exist *in vivo*. Meanwhile, there is higher concentration of Vc in the blood and the reduction of nitroxide radicals into the corresponding hydroxylamines by GSH is much slower than Vc.[51] Thus, we compared the reduction resistance of TEMPO radicals embedded in the TEMPO@SiO_2 nanoparticles with the free TEMPO radicals in the presence of antioxidant Vc.

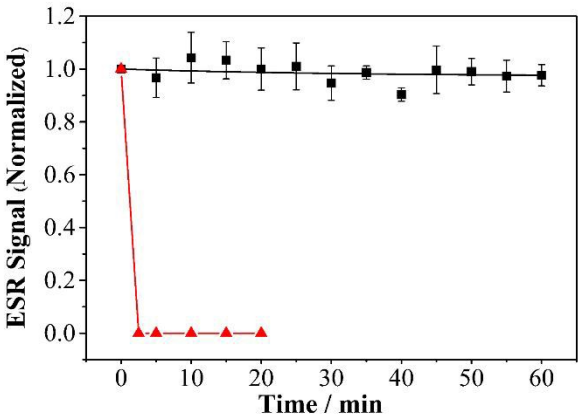

Fig. 1 Time-course of ESR signal intensity of TEMPO@SiO_2 nanoparticles (■) and 4-hydroxyl-TEMPO (▲) in the prescence of 5 mM ascorbic acid. (Preformed in 20 mM pH 7.4 Tris-HCl buffer solution, [4-hydroxyl-TEMPO] = 10 mM, TEMPO@SiO_2 nanoparticles: 7 mg/mL).

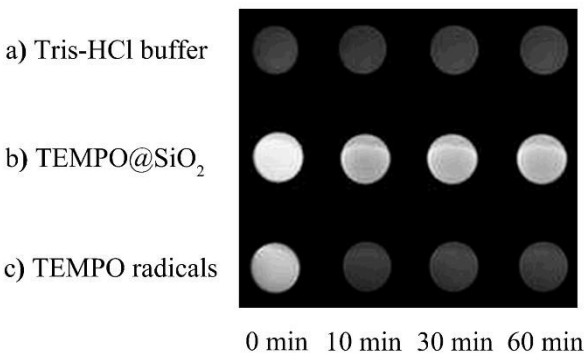

Fig. 2 Time-course of T_1-weighted MR images for a) Tris-HCl buffer control, b) TEMPO@SiO_2 nanoparticles and c) 4-hydroxyl-TEMPO in the present of 5 mM ascorbic acid. (Performed in 20 mM pH 7.4 Tris-HCl buffer solution, [4-hydroxyl-TEMPO] = 1 mM, TEMPO@SiO_2 nanoparticles: 7 mg/mL.)

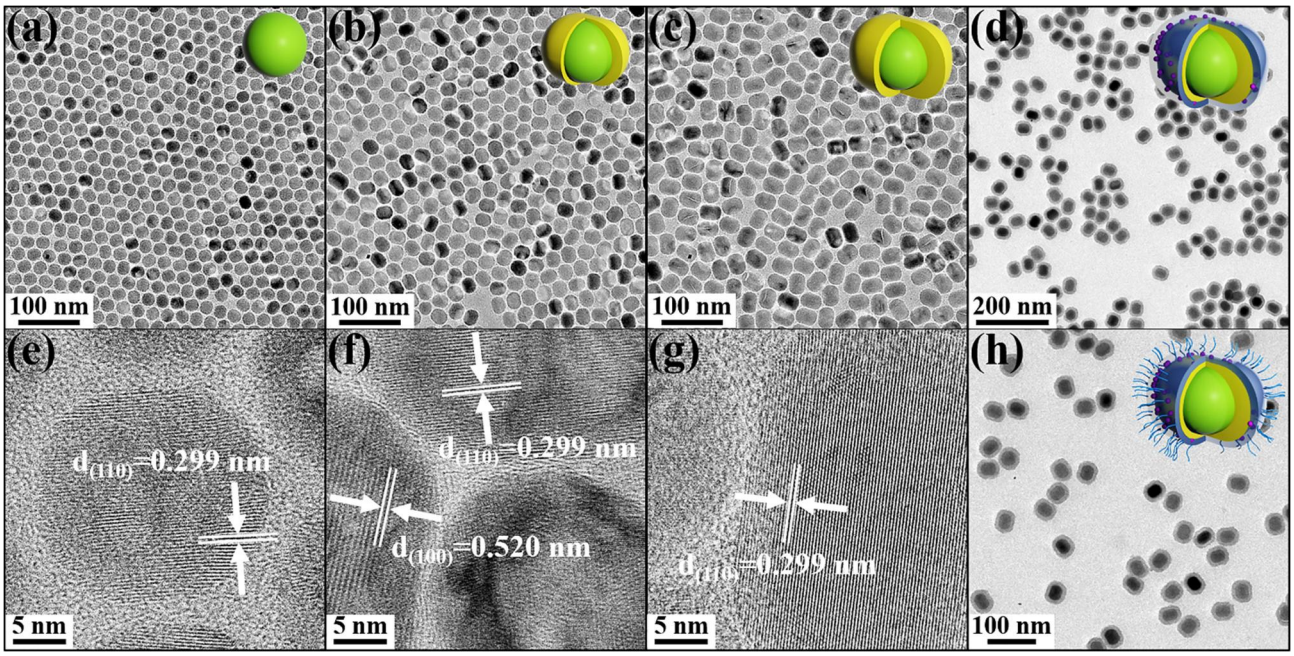

Fig. 3 TEM images of core $NaYF_4$:Yb,Er nanoparticles (a), core-shell $NaYF_4$:Yb,Er/$NaYF_4$ nanoparticles with 15 (b) and 30 (c) layers of $NaYF_4$ shell, UCNP@TEMPO@SiO_2 nanocomposites (d) and PEGylated UCNP@TEMPO@SiO_2 nanocomposites (h). (e) – (g) show the corresponding HRTEM images of (a) – (c), respectively.

The time-course of ESR signal intensity of TEMPO@SiO_2 nanoparticles and free TEMPO radicals is shown in Fig. 1. The ESR signal of the as-prepared TEMPO@SiO_2 was not significantly affected by ascorbic acid up to concentration of 5 mM while the signal intensity of free TEMPO radicals decreased rapidly within about 1 min. These results indicate that the compact network structure of SiO_2 could act as both the protector and promising carrier of nitroxide radicals, the compartmentalization of the TEMPO radicals in the microstructure of SiO_2 nanoparticle is an effective way to maintain their ESR signal, especially in reduction environment.

In addition, the reduction resistance of TEMPO@SiO_2 was also confirmed by time-course MRI. The time-course of T_1-weighted MR images of TEMPO@SiO_2 nanoparticles and free TEMPO radicals under reduction environment are shown in Fig. 2. Compared with the Tris-HCl buffer blank control, both of TEMPO@SiO_2 nanoparticles and free TEMPO radicals showed significant contrast enhancement of T_1-weighted MRI in Tris-HCl solution containing Vc (5 mM) at the very start. By virtue of compact network structure of SiO_2, the TEMPO radicals embedded in TEMPO@SiO_2 nanoparticles could resist reduction for 1 h, while the contrast enhancement of free TEMPO radicals decreased quickly within 10 min, ascribing to the reduction by Vc.

3.2 One-pot synthesis and characterization of core $NaYF_4$:Yb,Er and core-shell $NaYF_4$:Yb,Er/$NaYF_4$ UCNPs

TEM images of core $NaYF_4$:Yb,Er and core-shell $NaYF_4$:Yb,Er/$NaYF_4$ nanoparticles are shown in Fig. 3. All of these nanoparticles were orderly self-assembled on TEM grid easily (Fig. S6†). As can be seen in Fig. 3 (a), the core $NaYF_4$:Yb,Er nanoparticles are uniform and nearly spherical in shape with an average diameter of 19.6 ± 1.1 nm. The morphology of the resulting core-shell $NaYF_4$:Yb,Er/$NaYF_4$ nanoparticles coated with 15 layers (Fig. 3b) and 30 layers (Fig. 3c) of $NaYF_4$ shell became ellipsoidal in shape with narrow size distribution and the average size increased from 19.6 ± 1.1 nm (core size) to 27.2 ± 1.1 nm (length) × 21.7 ± 0.9 nm (width) and 33.4 ± 1.2 nm × 25.1 ± 1.1 nm, respectively. Meanwhile, the corresponding high-resolution TEM (HRTEM) images of core $NaYF_4$:Yb,Er (Fig. 3e) and core-shell $NaYF_4$:Yb,Er/$NaYF_4$ (Fig. 3f and g) reveal the high crystallinity of these nanoparticles. The distance between lattice fringes were 0.520 nm and 0.299 nm, consistent with the (100) and (110) lattice planes of hexagonal-phase $NaYF_4$ structure, respectively. All core and core-shell samples were further determined as hexagonal phase $NaYF_4$ by XRD (Fig. S9†) and SAED (Fig. S10†). This shape variation from spherical to ellipsoidal nanoparticles further confirms the successively epitaxial growth of an inert $NaYF_4$ layer due to anisotropic shell growth (Fig. S7†). It can therefore be concluded from these observations that the growth of $NaYF_4$ shell on core $NaYF_4$:Yb,Er is highly anisotropic (Fig. S8†). In addition, the approximative volume ratio of core $NaYF_4$:Yb,Er to outer $NaYF_4$ shell is 1:3.19. This value is well consistent with the molar ratio of the precursors of lanthanide input (1:3) for generating the core and shell components, respectively (The detail geometric structures analysis is presented in the ESI†).

Upconversion luminescence (UCL) spectra of core $NaYF_4$:Yb,Er nanoparticles and core-shell $NaYF_4$:Yb,Er/$NaYF_4$ nanoparticles are shown in Fig. 4. Under 980nm laser excitation, a set of upconversion emissions centered at 379 nm, 410 nm, 521 nm, 542 nm and 651 nm are observed, corresponding to $^4G_{11/2}\rightarrow{}^4I_{15/2}$ (379 nm), $^2H_{9/2}\rightarrow{}^4I_{15/2}$ (410 nm), $^2H_{11/2}\rightarrow{}^4I_{15/2}$ (521 nm), $^4S_{3/2}\rightarrow{}^4I_{15/2}$ (542 nm), and $^4F_{9/2}\rightarrow{}^4I_{15/2}$ (651 nm) transitions of Er^{3+} ions, respectively.[52] The total integrated UCL intensity of core-shell $NaYF_4$:Yb,Er/$NaYF_4$ nanoparticles with successive shell growth showed an obvious enhancement, even up to a factor of about 60 times for the core-shell $NaYF_4$:Yb,Er/$NaYF_4$ nanoparticles with 30 layers of $NaYF_4$ shell (Fig. S11†). This result suggests that epitaxial growth of multiple inert $NaYF_4$ shell on the core $NaYF_4$:Yb,Er nanoparticles can effectively minimize the luminescence quenching from the imperfections located at the core particle surface and the surrounding ligands and solvents with high phonon energy.[53]

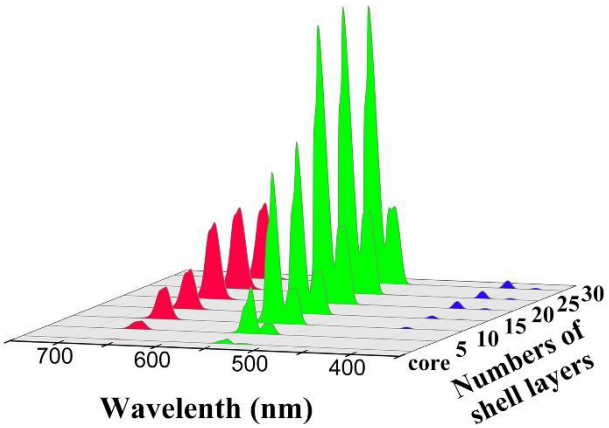

Fig. 4 Upconversion emission spectra of the core $NaYF_4$:Yb,Er and core−shell $NaYF_4$:Yb,Er/$NaYF_4$ UCNPs with different layers of inner $NaYF_4$ shell at same concentration (1 mg/mL) in cyclohexane under 980 nm excitation (power 0.1 W).

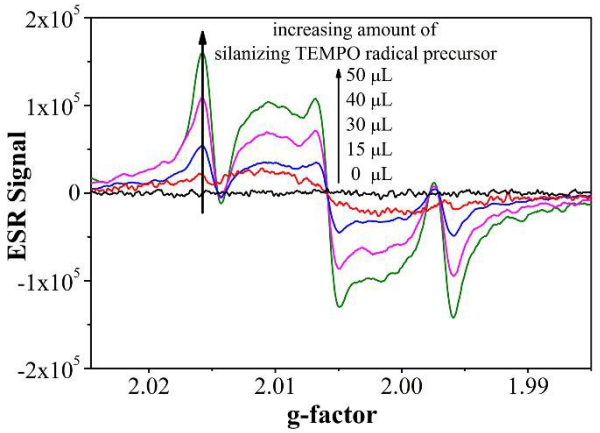

Fig. 5 The ESR spectra recorded in aqueous solution of the UCNP@TEMPO@SiO_2 nanocomposites synthesized with variable amounts of silanizing TEMPO radical precursors added during the process of copolymerization.

Compared with the one-pot successive layer-by layer (LBL) thermal decomposition method developed by Zhao et al. (the molar concentration ratio of F^-/Ln^{3+} ions is 6:1)[54] and Chen et al. (the molar concentration ratio of F^-/Ln^{3+} ions is 12:1),[55] it has to be mentioned that we still choose a stoichiometric amount of NaOH and NH_4F mixed with lanthanide-oleate coordination complexes in OA/ODE dispersion as the shell precursor (the molar concentration ratio of F^-/Ln^{3+} ions is 4:1), owing to some safety concerns about the HF gas or toxic fluorinated species produced by the pyrolysis of excessive fluoride reactants (CF_3COONa, $(CF_3COO)_3Re$, etc.) at high temperatures. By this user-friendly one-pot solvothermal strategy using NH_4F-NaOH-Re-OA as shell precursors, the injection could be easily performed to more than 50 cycles to prepare hierarchical uniform core–shell UCNPs, without worrying about excess amounts of fluoride reactants in high temperature reaction.

3.3 Synthesis and characterization of PEGylated UCNP@TEMPO@SiO_2 nanocomposites

Inspired by the high reduction resistance of TEMPO@SiO_2 against reducing environment, we further developed a hybrid nanocomposite by using core-shell $NaYF_4$:Yb,Er/$NaYF_4$ (30 layers) UCNPs as core and the TEMPO@SiO_2 as shell, which could maintain the ESR signal under reducing conditions for a long time when these nanocomposites were used in UCL/MR dual-modality imaging. At the same time, the TEMPO@SiO_2 would serve as a hydrophilic shell to make the hydrophobic $NaYF_4$:Yb,Er/$NaYF_4$ UCNPs dispersible in aqueous solution and easy for the functionalization with various biomolecules. TEM image of the $NaYF_4$:Yb,Er/$NaYF_4$ nanoparticles coated with TEMPO@SiO_2 shell is shown in Fig. 3d. It confirms the successful preparation of monodisperse UCNP@TEMPO@SiO_2 nanocomposites. The thickness of TEMPO@SiO_2 shell was about 10 nm. The narrow size distribution also indicate the uniform morphology of UCNP@TEMPO@SiO_2 nanocomposites (length: 51.8 ± 1.6 nm, width: 43.9 ± 1.7 nm). X-ray photoelectron (XPS) spectra analysis provides detailed information on the chemical composition of UCNP@TEMPO@SiO_2 nanocomposites (Fig. S12†). The wide scan spectrum indicates the presence of Si, Y, C, N, O, F and Na elements in UCNP@TEMPO@SiO_2 nanocomposites. These chemical composition were also confirmed by EDX analysis (Fig. S13†).

Then, the obtained UCNP@TEMPO@SiO_2 nanocomposites were transferred to a capillary tube, followed by ESR measurement. As shown in Fig. 5, the ESR lines of UCNP@TEMPO@SiO_2 nanocomposites were extensively broader than that of TEMPO@SiO_2 nanoparticles. The mobility restriction accompanying with the bounding of TEMPO radicals to UCNPs@SiO_2 may contribute to the broadening of the ESR spectra. On the other hand, the ESR signal of UCNP@TEMPO@SiO_2 nanocomposites gradually enhanced with the increasing of the loading content of TEMPO radicals in the SiO_2 shell. The DLS data of UCNP@TEMPO@SiO_2 nanocomposites indicates that these nanoparticles are uniform in size and well dispersed in aqueous solution (Fig. S14†). A slightly increase of the hydrodynamic size could be caused by the increase in amount of the silanizing TEMPO radical precursors added during the process of copolymerization. Then, APTS was used to further modify the surface of UCNP@TEMPO@SiO_2 to provide active amino-groups for the graft of PEG or target molecules. In order to improve biocompatibility and extend blood circulation time, mPEG-NHS was immobilized to the surface of UCNP@TEMPO@SiO_2-NH_2. Note that the PEG derivative modification on the outermost surface of UCNP@TEMPO@SiO_2 has no obvious effect on the morphology and size of the nanocomposites, as has been presented in the corresponding TEM images (Fig. 3d and h). However, these surface modifications can substantially affect surface zeta potentials of the involved nanocomposites (Fig. S15†). The UCNP@TEMPO@SiO_2 nanocomposites initially hold a zeta potential of -36.1 mV. After modifying by APTS, the zeta potential increased to +27.2 mV, and then reduced to +22.8 mV after PEGylation. The reverse of zeta potential from negative to positive is attributed to the introduction of positive primary amine groups, however the decrease of zeta potential from +27.2 mV to +22.8 mV is attributed to the consumption of positive amine groups on the surface of the nanocomposites during the PEGylation process. Furthermore, the hydrodynamic diameter of the UCNP@TEMPO@SiO_2-PEG (78.8 nm) is larger than that of UCNP@TEMPO@SiO_2 (60.8 nm), which was attributed to the formation of protective layers of PEG bound covalently to the surface of the UCNP@TEMPO@SiO_2. The obtained PEGylated UCNP@TEMPO@SiO_2 nanocomposites can be well dispersed in serum for 24 h at 37 °C (data not shown), which will extend their blood circulation time.

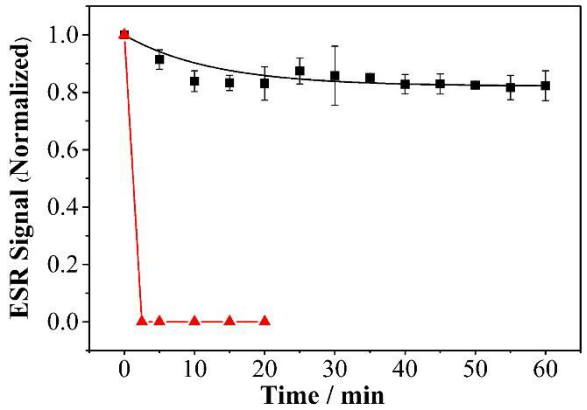

Fig. 6 Time-course of ESR signal intensity of UCNP@TEMPO@SiO_2 nanocomposites (■, 15 mg/mL, synthesized with 50 μL silanizing TEMPO radical precursors) and 4-hydroxyl-TEMPO (▲, 10 mM) in the prescence of 5 mM ascorbic acid. (Preformed in 20 mM pH 7.4 Tris-HCl buffer solution).

In order to test whether the multifunctional nanoprobes can maintain a satisfied paramagnetic property in reduction environment, we evaluated the reduction resistance capacity of PEGylated UCNP@TEMPO@SiO_2 nanocomposites in the presence of ascorbic acid. The time-course of ESR signal intensity of the as-prepared PEGylated UCNP@TEMPO@SiO_2 nanocomposites and free TEMPO radicals are shown in Fig. 6. When the free TEMPO radicals solution was monitored in the presence of 5 mM ascorbic acid, the signal intensity rapidly decreased within a minute. On the contrary, the ESR signal intensity of the PEGylated UCNP@TEMPO@SiO_2 nanocomposites maintained at a stable level for more than 60 min, indicating that the TEMPO radicals in PEGylated UCNP@TEMPO@SiO_2 nanocomposites resisted reduction even in the presence of 5 mM ascorbic acid. High stability of the TEMPO radicals in nanocomposites system means that signal will be observed in a long time and this nanocomposites are promising as new multifunctional nanoprobes for UCL/MR dual-modality imaging.

In order to assess the feasibility of the as-prepared nanocomposites for bioimaging applications, the upconversion luminescence (UCL) spectra of (a) core-only and (b) core-shell UCNPs in cyclohexane, (c) UCNP@SiO_2 nanocomposites and (d) PEGylated UCNP@TEMPO@SiO_2 nanocomposites in deionized water, are shown in Fig. 7. Here the UCNP refers to the core-shell $NaYF_4$:Yb,Er/$NaYF_4$ (30 layers). All of the spectra were obtained with same concentration of Yb^{3+} in sample solution as measured by ICP-AES. Compared with the core-shell UCNPs in cyclohexane, the UCL intensity of UCNP@SiO_2 nanocomposites dropped around 65% upon dispersing them into water. As the effect of silica coating on UCL intensity of UCNPs is very low or undetectable in most cases,[56] the obviously decrease of UCL intensity from (b) to (c) is mainly attributed to H_2O solvent effect. H_2O molecules can be regarded as a surface oscillator, due to their high energy vibration modes (~3600 cm^{-1}).[53, 57, 58] The interaction between the oscillator and the doped lanthanide ions can produce an increased nonradiative relaxation of excited states and thus results in the quenching of the UCL intensity. The 30 layers of inner $NaYF_4$ shell has modest effect on this quenching phenomenon. Although the inevitable decrease of UCL intensity was found when transfer the hydrophobic UCNPs from cyclohexane to aqueous solution, the PEGylated UCNP@TEMPO@SiO_2 nanocomposites still maintain a strong UCL emission in aqueous solution (as shown in Fig. 7). These results indicate that the PEGylated UCNP@TEMPO@SiO_2 nanocomposites show promising potential for NIR excited bioimaging applications.

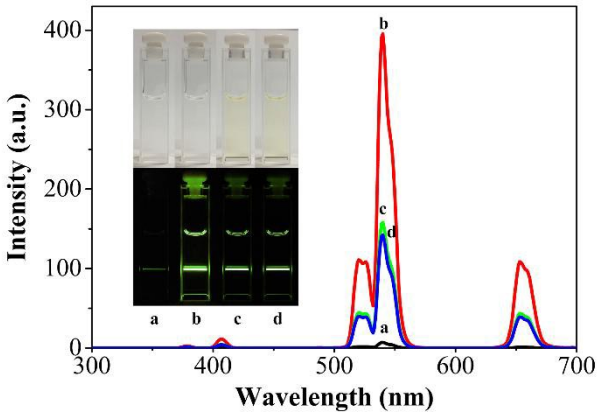

Fig. 7 Upconversion luminescence spectra of (a) core $NaYF_4$:Yb,Er and (b) core−shell $NaYF_4$:Yb,Er/$NaYF_4$ in cyclohexane, (c) UCNP@SiO_2 nanocomposites and (d) PEGylated UCNP@TEMPO@SiO_2 nanocomposites in deionized water. Here the UCNP refers to the core-shell $NaYF_4$:Yb,Er/$NaYF_4$ (30 layers). The inset shows the photographs of the upconversion emission of the corresponding solution in the daylight (top) and in the dark (bottom) under excitation of 980 nm (power 0.6 W), respectively.

3.4 *In vitro* cytotoxicity test and cellular uptake of PEGylated UCNP@TEMPO@SiO_2 nanocomposites

The cytotoxicity of PEGylated UCNP@TEMPO@SiO_2 nanocomposites was tested in HeLa cells based on MTT assay. The cell viability is not significantly affected by the nanocomposites up to concentration of 400 μg/mL (Fig. 8). These data show satisfactory results that the PEGylated UCNP@TEMPO@SiO_2 nanocomposites can serve as promising nanoprobes with low cytotoxicity for UCL/MR dual-modality imaging. The cellular uptake efficiency of PEGylated UCNP@TEMPO@SiO_2 nanocomposites were investigated by using flow cytometry and inverted fluorescence imaging microscope. Firstly, FITC was covalently bound to the surface of PEGylated UCNP@TEMPO@SiO_2 nanocompisites, then the cellular uptake degree of the nanocomposites was quantified with flow cytometry by determining the green fluorescence signal of FITC. As revealed by Fig. 9, PEGylated UCNP@TEMPO@SiO_2-FITC nanocomposites were taken up by HeLa cells relative to the controlled cells, and the cellular uptake of samples increases gradually with the increasing concentration of PEGylated UCNP@TEMPO@SiO_2-FITC nanocomposites (0, 8, 15, 30, 60, 125 μg/mL).

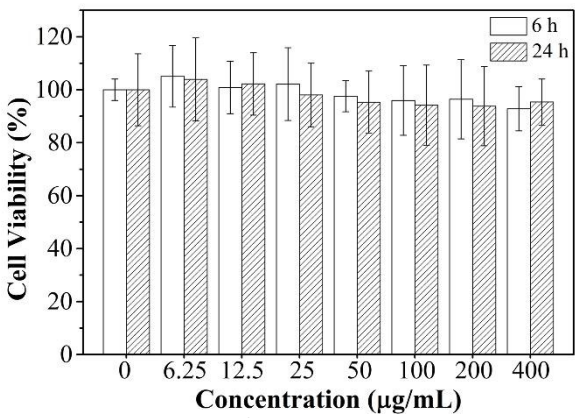

Fig. 8 *In vitro* cell viability of HeLa cells incubated with PEGylated UCNP@TEMPO@SiO_2 nanocomposites at different concentrations (0, 6.25, 12.5, 25, 50, 100, 200 and 400 μg/mL) for 6 h and 24 h at 37 °C.

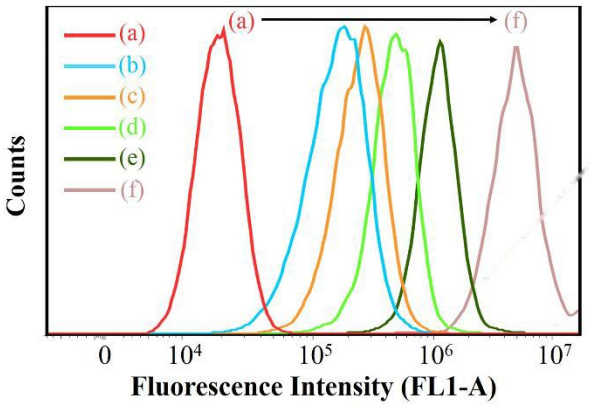

Fig. 9 Flow cytometry analysis of the HeLa cells incubated with PEGylated UCNP@TEMPO@SiO_2-FITC nanocomposites at different concentrations. (a) 0 μg/mL, as a control, (b) 8 μg/mL, (c) 15 μg/ml, (d) 30 μg/mL, (e) 60 μg/mL, (f) 125 μg/mL. Incubation time was 6 h.

Besides this, in order to further verify that PEGylated UCNP@TEMPO@SiO_2 nanocomposites can be internalized by the cells, the UCL imaging was done by utilizing a modified inverted fluorescence microscopy equipped with infrared laser excitation at 980 nm. After PEGylated UCNP@TEMPO@SiO_2 nanocomposites (200 μg/mL) were incubated with HeLa cells at 37 °C for 6 h, the strong upconversion luminescence signal can be observed from the HeLa cells without any cell auto-fluorescence (Fig. 10). Meanwhile, an increasing amount of PEGylated UCNP@TEMPO@SiO_2 nanocomposites were internalized into the cells as increasing the initial concentration of samples (Fig. S16†). These results indicate that PEGylated UCNP@TEMPO@SiO_2 nanocomposites can be used as an excellent luminescence probe for cellular labeling and cell imaging.

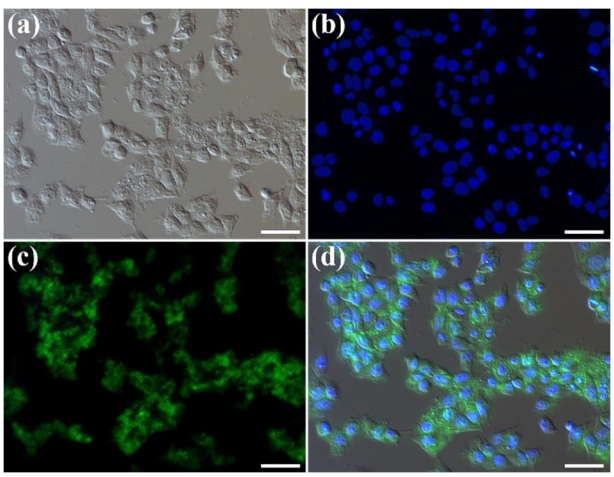

Fig. 10 Inverted fluorescence microscope images of HeLa cells incubated with PEGylated UCNP@TEMPO@SiO_2 nanocomposites at 200 μg/mL for 6 h at 37 °C. (a) Bright-field image, (b) nuclei of cells (being dyed in blue by Hoechst 33258 for visualization), (c) upconversion luminescence (UCL) image collected at green channel (500 nm to 600 nm), (d) the overlay image of three. All scale bar are 50 μm. All images were taken under the identical conditions and the nuclei was stained with Hoechst 33258.

3.5 MR relaxivity properties *in vitro* and MRI *in vivo*

The coating of TEMPO@SiO_2 to $NaYF_4$:Yb,Er/$NaYF_4$ nanoparticles not only make the UCNPs dispersible in aqueous solution and easy for the functionalization with various biomolecules, but also serve the nanocomposites as a contrast agent for T_1-weighted MR imaging due to the stable paramagnetic signal from TEMPO radical. In order to evaluate the feasibility of PEGylated UCNPs@TEMPO@SiO_2 nanocomposites as a MRI contrast agent, the r_1 relaxivity and corresponding T_1-weighted MR images of PEGylated UCNP@TEMPO@SiO_2 nanocomposites in water were measured on a 9.4 T MRI scanner.

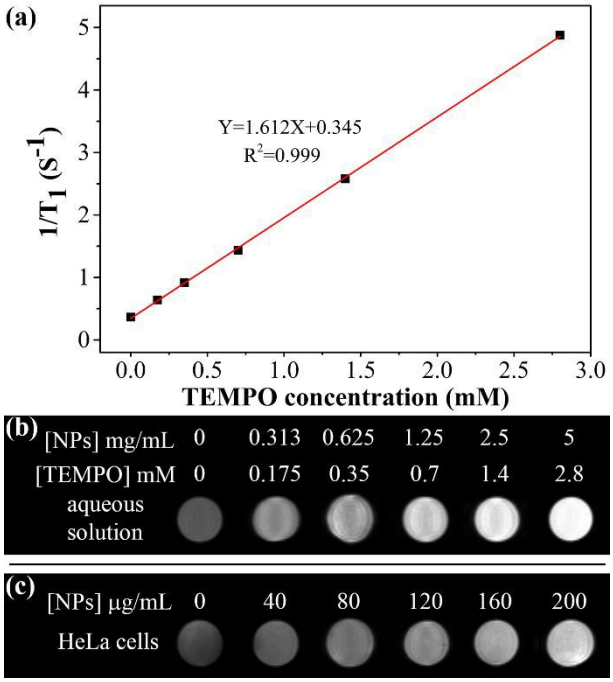

Fig. 11 (a) T_1-weighted relaxation rates ($1/T_1$, s^{-1}) and (b) T_1-weighted MR images of PEGylated UCNP@TEMPO@SiO_2 nanocomposites (NPs) as a function of [TEMPO radical] concentration (mM) in aqueous solution (9.4 T, 25 °C). (c) T_1-weighted MR images of the HeLa cells treated with PEGylated UCNP@TEMPO@SiO_2 nanocomposites at different concertrations (0, 40, 80, 120, 160 and 200 μg/mL) for 6 h at 37 °C.

As shown in Fig. 11, PEGylated UCNP@TEMPO@SiO_2 nanocomposites exhibited an enhanced signal intensity with a dose-dependent effect. The images become brighter with increased concentration of PEGylated UCNPs@TEMPO@SiO_2 nanocomposites in aqueous solution. The longitudinal relaxivity value (r_1) of PEGylated UCNPs@TEMPO@SiO_2 nanocomposites was estimated to be 1.61 $s^{-1}mM^{-1}$. The concentration of TEMPO radicals was determined by measuring the absorption of TEMPO radicals at 436 nm with a molar absorptivity coefficient of 13.3 $dm^3\ mol^{-1}\ cm^{-1}$ (Fig. S17†). Details of the theoretical calculation are given in the ESI.† It is interesting to note that this relaxivity observed for PEGylated UCNPs@TEMPO@SiO_2 nanocomposites is about 10 times stronger than that for free TEMPO radicals (about 0.15 $s^{-1}mM^{-1}$) and it is impressive when compared with other nitroxide radical-based system.[41, 44, 59] The great enhancement of r_1 relaxivity is most probably attributed to the reduced tumbling rate of TEMPO radicals, thereby increasing the rotational correlation time of TEMPO.[60, 61] Moreover, it has been reported previously that the r_1 relaxivity of TEMPO radical was proportionally increased depending on the

number of paramagnetic centers in a molecule.[59, 62] Similarly, coupling of nitroxyl molecules in a paramagnetic silica network could also significantly enhance the T_1-weighted contrast performance of nitroxide radicals. In addition, if being calculated on a per millimolar particle basis, the nanocomposites can reach a remarkably high longitudinal relaxivity (r_1) since at least 10^4 nitroxide radicals have been doped within the compact network structure of SiO_2 shell of a single nanocomposite (The detail calculation formulae are presented in the ESI†). These results suggest that the PEGylated UCNPs@TEMPO@SiO_2 nanocomposites have the potential to serve as an efficient MRI contrast agent due to their high payloads of paramagnetic centers.

To validate the diagnostic potential of the PEGylated UCNP@TEMPO@SiO_2 nanocomposites used as an MRI probe in cell level, the MR signal intensity of the HeLa cells were measured after incubation with PEGylated UCNP@TEMPO@SiO_2 nanocomposites at different concentrations of 40, 80, 120, 160 and 200 μg/mL for 6 h at 37 °C. The T_1-weighted MR contrast of HeLa cells treated with PEGylated UCNP@TEMPO@SiO_2 nanocomposites was clearly enhanced when comparing with that of the control cells (Fig. 11c). These results indicate that the encapsulation of TEMPO radicals within the compact network structure of SiO_2 may be an efficient way to make a useful contrast agent for T_1-weight MR imaging.

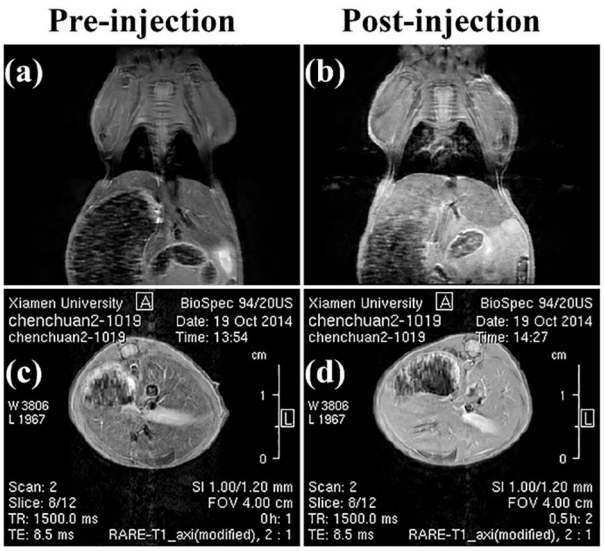

Fig. 12 *In vivo* T_1-weighted coronal MR images of the whole body (a, b) and the transversal cross-sectional images of the liver (c, d) of mice at pre-injection and at 30 min post-injection of PEGylated UCNP@TEMPO@SiO_2 nanocomposites.

To further demonstrate the performance of PEGylated UCNP@TEMPO@SiO_2 nanocomposites as a nanoprobe for *in vivo* MRI, the nanocomposites were intravenously injected into nude mice for MR imaging using a 9.4 T MR imaging system. Anatomical images were acquired in the coronal and transversal planes. Comparison of pre- and post-contrast T_1-weighted coronal MR images of the whole-body showed significant contrast enhancement in several organs, with the greatest enhancement in the liver of mice (Fig. 12a and b). For transversal cross-sectional images (Fig. 12c and d), significant contrast enhancement observed in the liver area further confirms the accumulation of these nanocomposites in liver. Because the liver is the main organ for eliminating foreign particles, rapid accumulation in the liver and relatively slow excretion are classical behaviors of nanocomposites *in vivo*.[63] These observations indicate that the present PEGylated UCNP@TEMPO@SiO_2 nanocomposites could circulate in the blood vessels without aggregation and were gradually cleared from reticuloendothelial systems such as liver.[14] These evidences of *in vivo* results indicate that PEGylated UCNP@TEMPO@SiO_2 nanocomposites could serve as a T_1-weighted MRI contrast agent in small-animal imaging. Compare with the IONP-UCNP nanocomposites and Gd-based UCNPs, the developed PEGylated UCNP@TEMPO@SiO_2 nanocomposties not only show a satisfactory MRI contrast ability but also maintain intense UCL emission. These unique properties will serve them as potential multifunctional nanoprobes for UCL/MR dual-modality imaging.

Conclusions

In summary, a novel class of PEGylated UCNP@TEMPO@SiO_2 multifunctional nanoprobes has been developed for UCL/MR dual-modality imaging. The presence of $NaYF_4$:Yb,Er/$NaYF_4$ UCNPs gives rise to intense upconversion emission for UCL imaging. The compact SiO_2 shell can protect the embedded TEMPO radicals from being reduced to the corresponding hydroxylamines in biological environment when compared with free radicals. The TEMPO@SiO_2 shell can provide the paramagnetic property and induce the enhancement of the positive-contrast of MR imaging. The cytotoxicity assay shows PEGylated UCNP@TEMPO@SiO_2 nanocomposites possess low toxicity. *In vitro* UCL imaging study confirms PEGylated UCNP@TEMPO@SiO_2 nanocomposites are well suited for cell imaging. The preliminary *in vivo* MRI results indicate PEGylated UCNP@TEMPO@SiO_2 nanocomposites can serve as T_1-weighted MRI contrast agents. Therefore, we expect that such multifunctional nanoprobe, combining the advantages of TEMPO-based paramagnetic MRI contrast agent and upconversion luminescence of core-shell $NaYF_4$:Yb,Er/$NaYF_4$ UCNPs, will find extensive applications in UCL/MR dual-modality bioimaging.

Acknowledgements

This work was financially supported by the National Basic Research Program of China (973 Program) (2011CB910403, 2013CB933703,) and the National Nature Science Foundation of China (NSFC grants 31371012 and 81171448).

Notes and references

[a] The MOE Key Laboratory of Spectrochemical Analysis and Instrumentation, State Key Laboratory of Physical Chemistry of Solid Surfaces, Department of Chemistry, College of Chemistry and Chemical Engineering, Xiamen University, Xiamen 361005, P. R. China.

[b] Department of Biomaterials, College of Materials, Xiamen University, Xiamen 361005, P. R. China.

* Corresponding author. E-mail: xqguo@xmu.edu.cn (X. Q. Guo); renlei@xmu.edu.cn (L. Ren); Tel: +86 0592 2181682; Fax: +86 0592 2181682.

† Electronic supplementary information (ESI) available: ESI-MS spectrum, TEM image and ESR spectra of the silanizing nitroxide radical precursor and TEMPO@SiO_2 nanoparticles. Schematic illustration of the paramagnetic SiO_2 network formation. TEM images and size distribution of the core and core-shell UCNPs. Schematic of anisotropic shell growth of $NaYF_4$ shell on the core $NaYF_4$:Yb,Er. XRD spectra and SAED pattern of UCNPs. XPS spectrum, EDX analysis, DLS size distribution and Zeta potential of UCNP@TEMPO@SiO_2 nanocomposites. Inverted fluorescence microscope images of HeLa cells incubated with nanocomposites. UV-vis spectra of nanocomposites. Geometric structure analysis of UCNPs and the calculation of molar TEMPO radical : molar UCNP ratio. See DOI: 10.1039/b000000x/

1. J. Kim, Y. Piao and T. Hyeon, *Chem. Soc. Rev.*, 2009, **38**, 372-390.
2. A. Louie, *Chem. Rev.*, 2010, **110**, 3146-3195.
3. J. Yao, M. Yang and Y. X. Duan, *Chem. Rev.*, 2014, **114**, 6130–6178.
4. Y. I. Park, K. T. Lee, Y. D. Suh and T. Hyeon, *Chem. Soc. Rev.*, 2014, DOI: 10.1039/C4CS00173G.
5. L. N. Sun, Z. W. Wei, H. G. Chen, J. L. Liu, J. J. Guo, M. Cao, T. Q. Wen and L. Y. Shi, *Nanoscale*, 2014, **6**, 8878–8883.
6. L. N. Sun, T. Liu, Y. N. Qiu, J. L. Liu, L. Y. Shi and O. S. Wolfbeis, *Microchim. Acta*, 2014, **181**, 775–781.
7. L. Cheng, C. Wang and Z. Liu, *Nanoscale*, 2013, **5**, 23-37.
8. Z. W. Wei, L. N. Sun, J. L. Liu, J. Zhang, H. R. Yang, Y. Yang and L. Y. Shi, *Biomaterials*, 2014, **35**, 387–392.
9. S. L. Gai, C. X. Li, P. P. Yang and J. Lin, *Chem. Rev.*, 2014, **114**, 2343–2389.
10. L. Cheng, K. Yang, Y. G. Li, J. H. Chen, C. Wang, M. W. Shao, S. T. Lee and Z. Liu, *Angew. Chem., Int. Ed.*, 2011, **50**, 7385–7390.
11. W. Feng, C. M. Han and F. Y. Li, *Adv. Mater.*, 2013, **25**, 5287–5303.
12. Y. Sun, X. J. Zhu, J. J. Peng and F. Y. Li, *ACS Nano*, 2013, **7**, 11290–11300.
13. R. Kumar, M. Nyk, T. Y. Ohulchanskyy, C. A. Flask and P. N. Prasad, *Adv. Funct. Mater.*, 2009, **19**, 853-859.
14. J. Zhou, M. X. Yu, Y. Sun, X. Z. Zhang, X. J. Zhu, Z. H. Wu, D. M. Wu and F. Y. Li, *Biomaterials*, 2011, **32**, 1148-1156.
15. Q. F. Xiao, X. P. Zheng, W. B. Bu, W. Q. Ge, S. J. Zhang, F. Chen, H. Y. Xing, Q. G. Ren, W. P. Fan, K. L. Zhao, Y. Q. Hua and J. L. Shi, *J. Am. Chem. Soc.*, 2013, **135**, 13041–13048.
16. D. L. Ni, W. B. Bu, S. J. Zhang, X. P. Zheng, M. Li, H. Y. Xing, Q. F. Xiao, Y. Y. Liu, Y. Q. Hua, L. P. Zhou, W. J. Peng, K. L. Zhao and J. L. Shi, *Adv. Funct. Mater.*, 2014, **24**, 6613–6620.
17. D. L. Ni, J. W. Zhang, W. B. Bu, H. Y. Xing, F. Han, Q. F. Xiao, Z. W. Yao, F. Chen, Q. J. He, J. N. Liu, S. J. Zhang, W. P. Fan, L. P. Zhou, W. J. Peng and J. L. Shi, *ACS Nano*, 2014, **8**, 1231–1242.
18. L. N. Sun, X. Q. Ge, J. L. Liu, Y. N. Qiu, Z. W. Wei, B. Tian and L. Y. Shi, *Nanoscale*, 2014, **6**, 13242-13252.
19. Y. Zhang, G. K. Das, V. Vijayaragavan, Q. C. Xu, P. Padmanabhan, K. K. Bhakoo, S. T. Selvan and T. T. Y. Tan, *Nanoscale*, 2014, **6**, 12609-12617.
20. B. Liu, C. X. Li, P. A. Ma, Y. Y. Chen, Y. X. Zhang, Z. Y. Hou, S. S. Huang and J. Lin, *Nanoscale*, 2014, DOI: 10.1039/C4NR05342G.
21. D. Wang, L. Ren, X. Zhou, X. Z. Wang, J. Zhou, Y. Han and N. Kang, *Nanotechnology*, 2012, **23**, 225705.
22. Y. Wang, L. Ji, B. B. Zhang, P. H. Yin, Y. Y. Qiu, D. Q. Song, J. Y. Zhou and Q. Li, *Nanotechnology*, 2013, **24**, 175101.
23. F. Chen, W. B. Bu, S. J. Zhang, X. H. Liu, J. N. Liu, H. Y. Xing, Q. F. Xiao, L. P. Zhou, W. J. Peng, L. Z. Wang and J. L. Shi, *Adv. Funct. Mater.*, 2011, **21**, 4285–4294.
24. Z. Q. Li and Y. Zhang, *Nanoscale*, 2010, **2**, 1240-1243.
25. A. Xia, M. Chen, Y. Gao, D. M. Wu, W. Feng and F. Y. Li, *Biomaterials*, 2012, **33**, 5394–5405.
26. S. L. Gai, P. P. Yang, C. X. Li, W. X. Wang, Y. L. Dai, N. Niu and J. Lin, *Adv. Funct. Mater.*, 2010, **20**, 1166–1172.
27. L. Cheng, K. Yang, Y. G. Li, X. Zeng, M. W. Shao, S. T. Lee and Z. Liu, *Biomaterials*, 2012, **33**, 2215–2222.
28. J. Berliner and H. Fujii, *Science*, 1985, **227**, 517-519.
29. Z. Zhelev, R. Bakalova, I. Aoki, K. Matsumoto, V. Gadjeva, K. Anzai and I. Kanno, *Mol. Pharmaceutics*, 2009, **6**, 504-512.
30. J. H. Ortony, C. J. Newcomb, J. B. Matson, L. C. Palmer, P. E. Doan, B. M. Hoffman and S. I. Stupp, *Nat. Mater.*, 2014, **13**, 812–816
31. A. Hahn, S. Reschke, S. Leimkuehler and T. Risse, *J. Phys. Chem. B*, 2014, **188**, 7077-7084.
32. L. B. Du, S. P. Huang, Q. F. Zhuang, H. Y. Jia, A. Rockenbauer, Y. P. Liu, K. J. Liu and Y. Liu, *Nanoscale*, 2014, **6**, 1646-1652.
33. K. Matsumoto, F. Hyodo, A. Matsumoto, A. P. Koretsky, A. L. Sowers, J. B. Mitchell and M. C. Krishna, *Clin. Cancer Res.*, 2006, **12**, 2455-2462.
34. F. Hyodo, K. Chuang, A. G. Goloshevsky, A. Sulima, G. L. Griffiths, J. B. Mitchell, A. P. Koretsky and M. C. Krishna, *J. Cereb. Blood Flow Metab.*, 2008, **28**, 1165-1174.
35. B. P. Soule, F. Hyodo, K. Matsumoto, N. L. Simone, J. A. Cook, M. C. Krishna and J. B. Mitchell, *Free Radical Biol. Med.*, 2007, **42**, 1632-1650.
36. K. Takechi, H. Tamura, K. Yamaoka and H. Sakurat, *Free Radical Res.*, 1997, **26**, 483-496.
37. T. Yoshitomi, D. Miyamoto and Y. Nagasaki, *Biomacromolecules*, 2009, **10**, 596-601.
38. T. Yoshitomi, R. Suzuki, T. Mamiya, H. Matsui, A. Hirayama and Y. Nagasaki, *Bioconjugate Chem.*, 2009, **20**, 1792-1798.
39. X. L. Zhuang, C. S. Xiao, K. Oyaizu, N. Chikushi, X. S. Chen and H. Nishide, *J. Polym. Sci., Part A: Polym. Chem.*, 2010, **48**, 5404-5410.
40. M. Gussoni, F. Greco, P. Ferruti, E. Ranucci, A. Ponti and L. Zetta, *New J. Chem.*, 2008, **32**, 323-332.
41. C. S. Winalski, S. Shortkroff, E. Schneider, H. Yoshioka, R. V. Mulkern and G. M. Rosen, *Osteoarthritis Cartilage*, 2008, **16**, 815–822.
42. M. C. Emoto, K. Yamada, M. Yamato and H. G. Fujii, *Neurosci. Lett.*, 2013, **546**, 11-15.
43. E. Tanimoto, S. Karasawa, S. Ueki, N. Nitta, I. Aoki and N. Koga, *RSC Adv.*, 2013, **3**, 3531-3534.
44. E. J. Rivera, R. Sethi, F. Qu, R. Krishnamurthy, R. Muthupillai, M. Alford, M. A. Swanson, S. S. Eaton, G. R. Eaton and L. J. Wilson, *Adv. Funct. Mater.*, 2012, **22**, 3691-3698.
45. H. C. Chan, K. Sun, R. L. Magin and H. M. Swartz, *Bioconjugate Chem.*, 1990, **1**, 32-36.
46. V. Muhr, Th. Hirsch, S. Wilhelm and O. S. Wolfbeis, *Acc. Chem. Res.*, 2014, **47**, 3481–3493.
47. C. Ghica and P. Ionita, *J. Mater. Sci.*, 2007, **42**, 10058-10064.
48. R. Ciriminna, J. Blum, D. Avnir and M. Pagliaro, *Chem.Commun.*, 2000, 1441.
49. C. Tansakul, E. Lilie, E. D. Walter, F. Rivera III, A. Wolcott, J. Z. Zhang, G. L. Millhauser and R. Braslau, *J. Phys. Chem. C*, 2010, **114**, 7793-7805.
50. E. Yoshida and T. Tanaka, *Colloid Polym. Sci.*, 2006, **285**, 135-144.
51. J. Fuchs, N. Groth, T. Herrling and G. Zimmer, *Free Radical Biol. Med.*, 1997, **22**, 967–976.
52. H. Dong, L. D. Sun and C. H. Yan, *Nanoscale*, 2013, **5**, 5703–5714.
53. G. Y. Chen, H. Ågren, T. Y. Ohulchanskyy and P. N. Prasad, *Chem. Soc. Rev.*, 2015, DOI: 10.1039/C4CS00170B.
54. X. M. Li, D. K. Shen, J. P. Yang, C. Yao, R. C. Che, F. Zhang and D. Y. Zhao, *Chem. Mater.*, 2013, **25**, 106-112.
55. P. Huang, W. Zheng, S. Y. Zhou, D. T. Tu, Z. Chen, H. M. Zhu, R. F. Li, E. Ma, M. D. Huang and X. Y. Chen, *Angew. Chem., Int. Ed.*, 2014, **53**, 1252-1257.
56. A. Sedlmeier, H. H. Gorris, *Chem. Soc. Rev.*, 2015, DOI: 10.1039/C4CS00186A.
57. J. C. Boyer, M. P. Manseau, J. I. Murray and F. C. J. M. van Veggel, *Langmuir*, 2010, **26**, 1157–1164.
58. F. Wang, J. Wang and X. G. Liu, *Angew. Chem., Int. Ed.*, 2010, **49**, 7456–7460.
59. K. Matsumoto, H. Yakumaru, M. Narazaki, H. Nakagawa, K. Anzai, H. Ikehira and N. Ikota, *Magn. Reson. Imaging*, 2008, **26**, 117-121.
60. J. Rudovský, M. Botta, P. Hermann, K. I. Hardcastle, I. Lukeš and S. Aime, *Bioconjugate chem*, 2006, **17**, 975-987.
61. S. Aime, M. Botta, M. Fasano, S. G. Crich and E. Terreno, *JBIC, J. Biol. Inorg. Chem.*, 1996, **1**, 312-319.
62. C. S. Winalski, S. Shortkroff, R. V. Mulkern, E. Schneider and G. M. Rosen, *Magn. Reson. Med.*, 2002, **48**, 965-972.
63. L. Q. Xiong, T. S. Yang, Y. Yang, C. J. Xu and F. Y. Li, *Biomaterials*, 2010, **31**, 7078–7085.

Table of contents

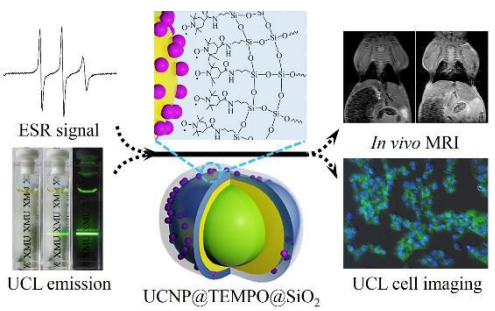

Nitroxide radicals doped SiO_2 nanostructure was synthesized and coated on upconversion nanoparticles to generate novel UCNP@TEMPO@SiO_2 nanoprobes for dual-modality imaging.